Nanoscale

PAPER

View Article Online
View Journal | View Issue

Cite this: *Nanoscale*, 2023, **15**, 10634

Experimental observation of the role of countercations in modulating the electrical conductance of Preyssler-type polyoxometalate nanodevices†

Cécile Huez, ‡[a] Séverine Renaudineau, [b] Florence Volatron, [b] Anna Proust *[b] and Dominique Vuillaume *[a]

Polyoxometalates are nanoscale molecular oxides with promising properties that are currently explored for molecule-based memory devices. In this work, we synthesize a series of Preyssler polyoxometalates (POMs), $[\mathrm{Na}\subset \mathrm{P_5W_{30}O_{110}}]^{14-}$, stabilized with four different counterions, H^+, K^+, NH_4^+, and tetrabutylammonium (TBA^+). We study the electron transport properties at the nanoscale (conductive atomic force microscopy, C-AFM) of molecular junctions formed by self-assembled monolayers (SAMs) of POMs electrostatically deposited on the ultraflat gold surface prefunctionalized with a positively charged SAM of amine-terminated alkylthiol chains. We report that the electron transport properties of P_5W_{30}-based molecular junctions depend on the nature of the counterions; the low-bias current (in the voltage range [−0.6 V; 0.6 V]) gradually increases by a factor of ~100 by changing the counterion in the order: K^+, NH_4^+, H^+ and TBA^+. From a statistical study (hundreds of current–voltage traces) using a simple analytical model for charge transport in nanoscale devices, we show that the energy position of the lowest unoccupied molecular orbital (LUMO) of P_5W_{30} with respect to the Fermi energy of the electrodes increases from ~0.4 eV to ~0.7 eV and that the electrode coupling energy also increases from ~0.05 to 1 meV in the same order from K^+, NH_4^+, H^+ to TBA^+. We discuss several hypotheses on the possible origin of these features, such as a counterion-dependent dipole at the POM/electrode interface and counterion-modulated molecule/electrode hybridization, with, in both cases, the largest effect in the case of TBA^+ counterions.

Received 2nd May 2023,
Accepted 21st May 2023

DOI: 10.1039/d3nr02035e

rsc.li/nanoscale

Introduction

Ions inserted (inadvertently or in a controlled way) into solid-state molecular junctions (MJs) play an important role in modulating or controlling the electron transport properties. For example, ions can modulate the conductance of MJs as theoretically predicted,[1,2] and as observed in several MJs, this conductance modulation depends on the chemical nature of the ions and the details of the molecule–ion conformation.[3–7] Not only the conductance of the MJs, but also the shape of the current–voltage (I–V) behavior can be *in situ* switched between a linear (symmetric) and a rectifying (asymmetric) behavior by inserting/removing the ions or moving the precise position (electrical field driven) of the ions in the MJs,[8–11] opening the way toward molecular-scale programmable functional devices and synaptic (neuro-inspired) behavior.[12,13] Polyoxometalates (POMs) are candidates of choice owing to their remarkable reversible multi-redox states[14,15] and photo-stimulable redox properties,[16,17] and they have attracted growing interest with several recent demonstrations of proof-of-principles such as silicon-integrated POM-based memory devices[18] and unconventional (in-memory and neuromorphic) computing devices.[19–21]

In solution, it is well known that the nature of counterions has a strong impact on the redox potentials for the POMs, and hence on the electron transfer rates.[22] In the specific case of POM-based molecular junctions, the interactions with un-

---

[a] *Institute for Electronics Microelectronics and Nanotechnology (IEMN), CNRS, University of Lille, Av. Poincaré, Villeneuve d'Ascq, France. E-mail: dominique.vuillaume@iemn.fr*

[b] *Institut Parisien de Chimie Moléculaire (IPCM), CNRS, Sorbonne Université, 4 Place Jussieu, Paris, France. E-mail: anna.proust@sorbonne-universite.fr*

† Electronic supplementary information (ESI) available: Synthesis details; IR and NMR characterization; fabrication of self-assembled monolayers; ellipsometry measurements; the protocol of C-AFM measurements; supplemental details on the I–V measurements (statistical data); details on the single energy level (SEL) model and on the statistical distribution of the model parameters; transition voltage spectroscopy (details on the technique and results); supplementary figures for the discussion. See DOI: https://doi.org/10.1039/d3nr02035e

‡ Now at: Instituto de Ciencia Molecular (ICMoL), University of Valencia, Spain.

avoidable counterions also control many properties of POM-based materials and devices.[23,24] For example, for a single POM on a metallic surface, the electron cloud density around the POM, as observed with a scanning tunneling microscope (STM), depends on the counterions that modify the hybridization between the POM and the metal surface.[25] A recent theoretical study shows that the presence of a counterion (whatever its nature, here tetramethylammonium (TMA) *vs.* Cs^+) moves the LUMO (lowest unoccupied molecular orbital) of $W_{18}O_{54}(SO_3)^{2-}$ based MJs closer to the Fermi energy of the electrodes (~0.08 eV above the Fermi energy in both the cases).[26] Despite this similar position of the LUMO, the computed current–voltage (*I–V*) curves showed slight differences in the shape (more asymmetric *I–V* with Cs^+). The authors suggest that this feature might be due to the small differences in the amplitude of the calculated transmission coefficient of electrons in the MJ, clearly calling for more joint experimental and theoretical work. They also noted that the presence of the counterions does not create additional new conduction channels in the MJs, but they modify the potential landscape "viewed" by the POMs that transmit the electrons through the junction.

Here, we synthesized a series of Preyssler polyoxometalates (POMs), $[Na{\subset}P_5W_{30}O_{110}]^{14-}$,[27] P_5W_{30} for short, stabilized with four different counterions, H^+, K^+, NH_4^+ and tetrabutylammonium ($N(C_4H_9)_4^+$ or TBA^+). We formed, by electrostatic deposition, monolayers of these POMs on an ultraflat Au surface prefunctionalized with a positively charged self-assembled monolayer (SAM) of amine-terminated alkylthiol chains following the protocol already developed and reported in our previous work for other POMs.[17,28] The electron transport (ET) properties of these POMs were measured by conductive-AFM (atomic force microscopy) and the current *vs.* voltage curves of these MJs were statistically analyzed (hundreds of *I–V* traces) to determine the energy position of the molecular orbitals involved in the ET and the electronic coupling between the molecules and the electrodes. We demonstrate that the energy position of the LUMO of P_5W_{30} with respect to the Fermi energy of the electrodes increases from ~0.4 eV to ~0.7 eV and that the electrode coupling energy evolves from ~0.05 to 1 meV depending on the nature of the counterion in the order of K^+, NH_4^+, H^+ and TBA^+.

Synthesis and structural characterization

The synthesis of the P_5W_{30} POMs with various counterions is schematized in Fig. 1a. The potassium salt of $[Na{\subset}P_5W_{30}O_{110}]^{14-}$ can be obtained under hydrothermal conditions.[29] The sample we used has the molecular formula $K_{13.3}Na_{0.7}[Na{\subset}P_5W_{30}O_{110}]\cdot27H_2O$. The ammonium salt $(NH_4)_{14}[Na{\subset}P_5W_{30}O_{110}]\cdot25H_2O$ has been prepared according to ref. 30. The acid salt $H_{14}[Na{\subset}P_5W_{30}O_{110}]\cdot44H_2O$ was prepared by ion exchange of a solution of the potassium salt in a Dowex 50W-X8 proton exchange resin, following a published pro-

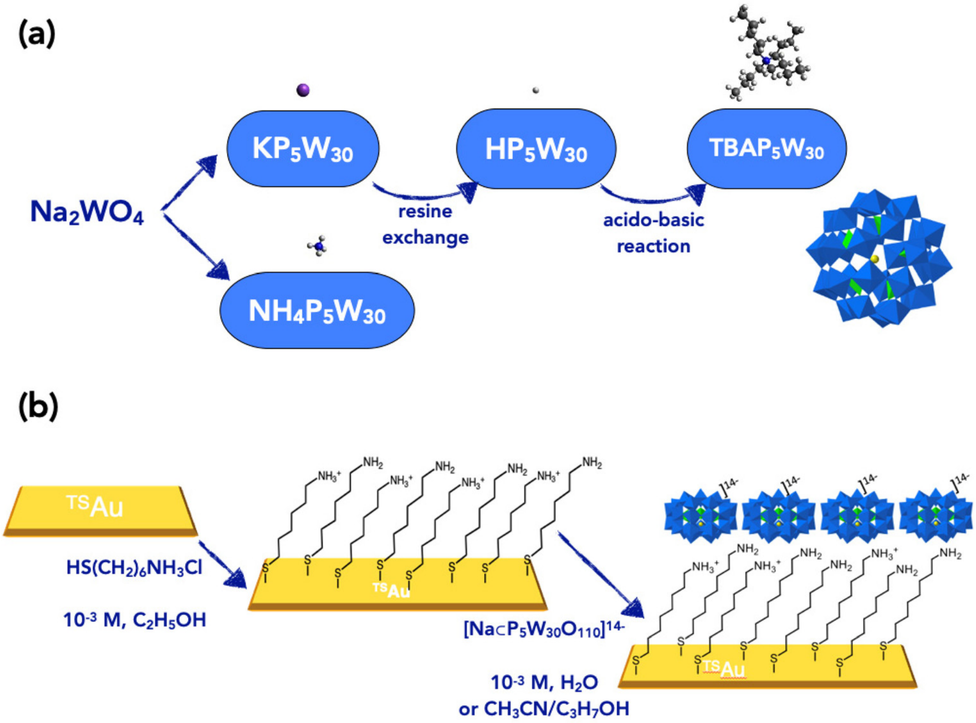

Fig. 1 (a) Schematic of the synthesis routes (cations and POM not at the scale). (b) Schematic description of the two-step fabrication of the self-assembled monolayers.

cedure.[31] Acido-basic titration of heteropolyacids with cation-hydroxides is a common route to introduce other cations and it has also been applied to this Preyssler-type phosphotungstic acid.[32] In our hands, the acido-basic titration of $H_{14}[Na\subset P_5W_{30}O_{110}]$ with tetrabutylammonium hydroxide was not complete, despite careful colorimetric monitoring of the equivalence. We ended up with the mixed salt $TBA_{10}H_4[Na\subset P_5W_{30}O_{110}]\cdot 24H_2O$.

We ended-up with 4 POMs: $K_{13.3}{}^{+}Na_{0.7}{}^{+}[Na\subset P_5W_{30}O_{110}]^{14-}$ (KP_5W_{30} for short); $H_{14}{}^{+}[Na\subset P_5W_{30}O_{110}]^{14-}$ (HP_5W_{30} for short); $TBA_{10}{}^{+}H_4{}^{+}[Na\subset P_5W_{30}O_{110}]^{14-}$ ($TBAP_5W_{30}$ for short) and $(NH_4)_{14}{}^{+}[Na\subset P_5W_{30}O_{110}]^{14-}$ ($NH_4P_5W_{30}$ for short). See more details, IR, ^{31}P NMR characterization, TGA and elemental analysis, in the ESI (Section 1†).

These POMs (dissolved in H_2O, or acetonitrile/isopropanol for HP_5W_{30} and $TBAP_5W_{30}$) were electrostatically deposited on ultra-flat template-stripped ^{TS}Au substrates functionalized with a 6-aminohexane-1-thiol hydrochloride ($HS–(CH_2)_6–NH_3{}^{+}/Cl^{-}$) self-assembled monolayer (SAM), or C6 SAM for short, following a protocol already developed and reported in our previous work for other POMs (Fig. 1b and also see Section 2 in the ESI†).[17,28] The thicknesses (systematically measured by ellipsometry, see Section 3 in the ESI†) are summarized in Table 1.

Table 1 Thickness measured by ellipsometry at each step of the fabrication of the molecular junction

Thickness (Å)	KP_5W_{30}	HP_5W_{30}	$NH_4P_5W_{30}$	$TBAP_5W_{30}$
C6-SAM			11 ± 2	
POM layer	9 ± 2	10 ± 2	9 ± 2	14 ± 2

We note that the P_5W_{30} POM has an oval shape with a long axis of 1.8 nm and a short axis of 1.3 nm. Thus the 1.4 nm measured thickness of the $TBAP_5W_{30}$ sample indicates a denser monolayer with possibly a small percentage of the $TBAP_5W_{30}$ molecule standing upright on the surface (vertical POM orientation), while the thinner values for the 3 other samples can be ascribed to a less compact monolayer regardless of the POM orientation (disordered monolayers with various POM orientations). The thicker $TBAP_5W_{30}$ SAM may also be caused by the bulky TBA ions (diameter ≈ 0.5–1 nm depending on the conformation of the butyl chains) mainly intercalated between the POMs and the electrode, while small cations can be distributed around the POM.

Electron transport properties

Fig. 2 shows the 2D-histograms (or "heat map") of the $I–V$ curves (between 400 and 500) acquired by C-AFM at different locations on the POM monolayer for the four $^{TS}Au–C6/POM//Pt$ MJs ("–" denotes a chemical bond, "/" electrostatic contact and "//" mechanical contact). The main feature is that these $I–V$ distributions have almost the same level of currents at large voltages, *i.e.* $|V| > 1$ V, while the currents in the voltage range [−0.6 V; 0.6 V] gradually increase with changing the counterion in the order from K^{+}, $NH_4{}^{+}$, H^{+} to TBA^{+}. This is clearly seen in Fig. 3a, showing the mean current–voltage ($\bar{I}–V$) plots for the 4

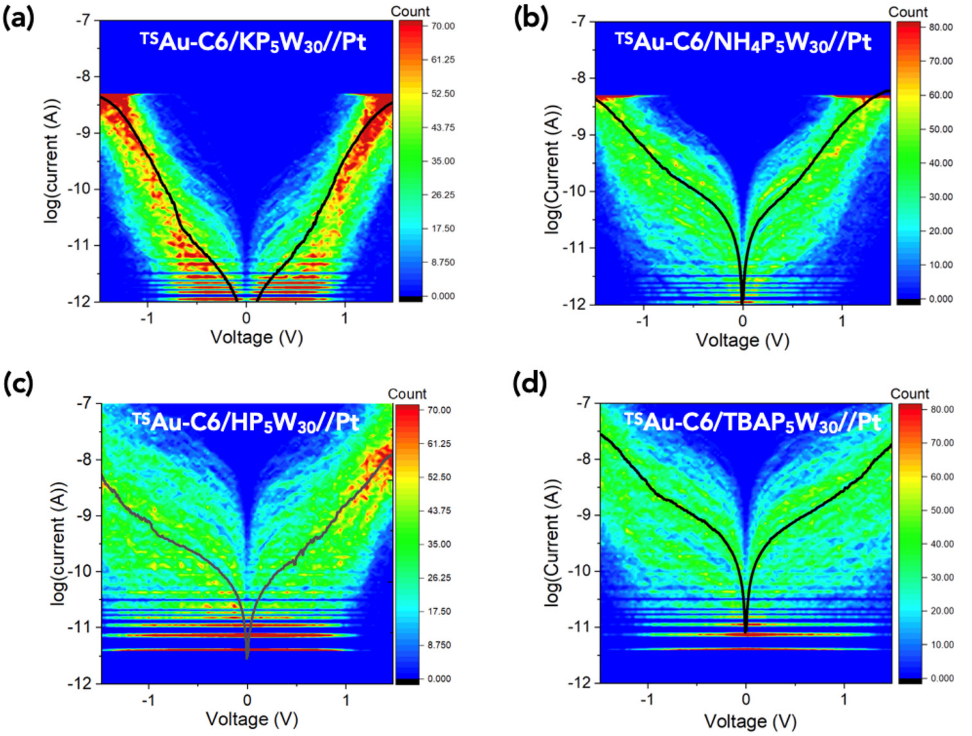

Fig. 2 2D histograms (400–500 $I–V$ traces) of the four samples in a semi-log$|I|–V$ plot. The solid black lines are the calculated mean $\bar{I}–V$ curves. (a) KP_5W_{30} MJs, (b) $NH_4P_5W_{30}$ MJs, (c) HP_5W_{30} MJs and (d) $TBAP_5W_{30}$ MJs.

samples and their counterion dependence at various voltages (Fig. 3b). The mean current $\bar{I}$ is around 10^{-8} A at ±1.5 V, while it varies over 2 decades at ±0.5 V. This observation is also supported by plotting and comparing the current histograms at given voltages (here at ±0.5 V and ±1 V), Fig. S9 and S10 in the ESI.†

The $\bar{I}$–V shapes for all samples show a bump at large voltages, *i.e.* $|V| > 0.7$–1 V, while the low-voltage $\bar{I}$–V's are well fitted between −0.6 and 0.6 V with a single-energy level (SEL) model given by the following analytical expression:[33,34]

$$I(V) = N\frac{8e}{h}\frac{\Gamma_1\Gamma_2}{\Gamma_1+\Gamma_2} \times \left[\arctan\left(\frac{\varepsilon_0+\frac{\Gamma_1}{\Gamma_1+\Gamma_2}\,\mathrm{eV}}{\Gamma_1+\Gamma_2}\right) - \arctan\left(\frac{\varepsilon_0-\frac{\Gamma_2}{\Gamma_1+\Gamma_2}\,\mathrm{eV}}{\Gamma_1+\Gamma_2}\right)\right] \tag{1}$$

where ε_0 is the energy of the molecular orbital (MO), here the LUMO, involved in the transport (with respect to the Fermi energy of the electrodes), Γ_1 and Γ_2 are the electronic coupling energies between the MO and the electron clouds in the two electrodes, e is the elementary electron charge, h is the Planck constant and N is the number of molecules contributing to the ET in the molecular junction (see details in Section 6 in the ESI†). Among several limitations (Section 6 in the ESI†), the SEL model is a low temperature approximation and the temperature broadening of the Fermi function in the electrodes is not taken into account. However, it was shown that it can be reasonably used at room temperature for voltages below the sharpened increase of the current (not observed here in the −0.6/0.6 V window) characterizing the transition between the off-resonance and resonant transport conditions at which the broadening of the Fermi function modifies the I–V shape.[35–37]

Fig. 3c shows typical examples of the SEL fits on the mean $\bar{I}$–V and Fig. 3d shows the evolution of the fitted parameters *versus* the nature of the counterions, clearly revealing an increase of the molecular energy level ε_0 from 0.42 eV (for KP_5W_{30}) to 0.69 eV (for $TBAP_5W_{30}$). The electrode coupling energies, Γ_1 and Γ_2, follow the same trend, increasing from ∼0.08 to 1–2 meV in the same counterion order (Fig. 3d and Table 2). The same trend is confirmed from a statistical analysis by fitting the SEL model with all the individual I–V's of the datasets shown in Fig. 2. The statistical distributions of ε_0, Γ_1 and Γ_2 for the 4 MJs are shown in Fig. S12 and S13 (ESI†) and the mean values of these distributions are summarized in Fig. 3d and Table 2.

The same results are obtained by analyzing the I–V curves with the transition voltage spectroscopy (TVS) method.[38–42] The energy level and the electrode coupling energy determined by the fit of the SEL model and by the TVS method are in very good agreement (Section 7, Fig. S14 and S15 in the ESI†).

Although the statistical analysis shows a large distribution of values (*e.g.* a factor ≈ 100 for the parameters Γ_1 and Γ_2 – Fig. S13 in the ESI,† and Table 2), the same trends and order

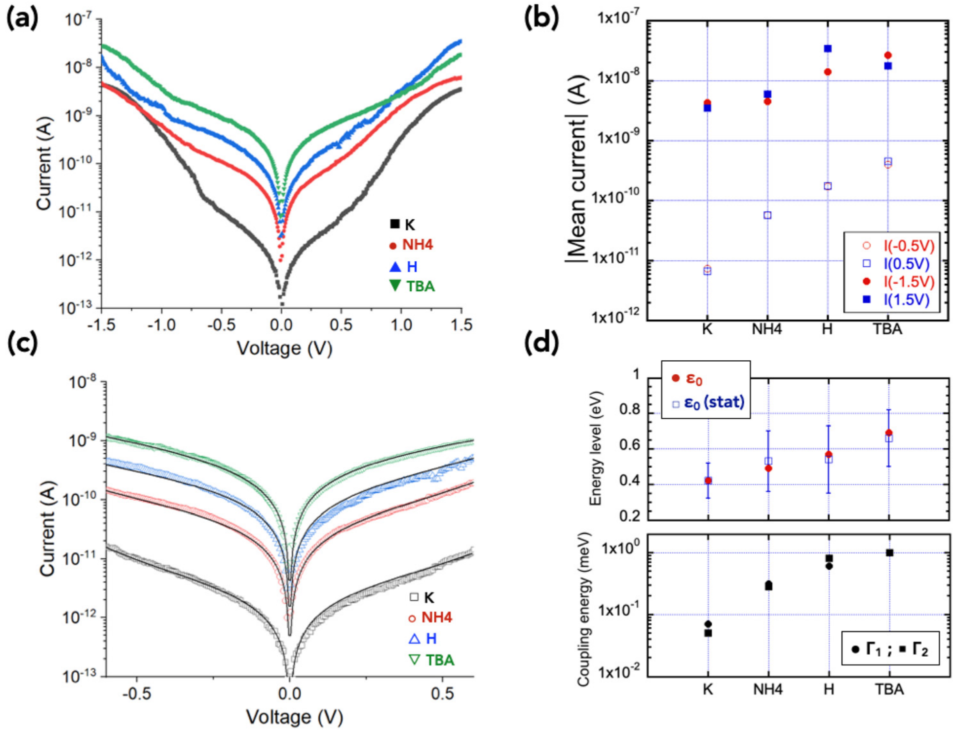

Fig. 3 (a) Mean $\bar{I}$–V curves for the four samples (from the datasets shown in Fig. 2), (b) counterion dependence of the mean current $\bar{I}$ at ±1.5 V and ±0.5 V, (c) fits (solid lines) of the SEL model in the voltage window [−0.6 V; 0.6 V] (fit R^2 = 0.995 for K^+, 0.998 for NH_4^+, 0.995 for H^+, 0.999 for TBA^+), (d) evolution of the SEL model parameters ε_0, Γ_1 and Γ_2 with the counterions.

Table 2 SEL parameters ε_0, Γ_1 and Γ_2 fitted on the mean $\bar{I}$–V (Fig. 3a) and mean values $\langle\varepsilon_0\rangle$, $\langle\Gamma_1\rangle$ and $\langle\Gamma_2\rangle$ deduced from the statistical analysis (see text). For the energy level $\langle\varepsilon_0\rangle$, the error is the standard deviation of the normal distribution (Fig. S12†). For the $\langle\Gamma_1\rangle$ and $\langle\Gamma_2\rangle$ parameters, the values in parentheses are the min and max values at the FWHM of the log–normal distributions (Fig. S13†)

	ε_0 (eV)	Γ_1 (meV)	Γ_2 (meV)	$\langle\varepsilon_0\rangle$ (eV)	$\langle\Gamma_1\rangle$ (meV)	$\langle\Gamma_2\rangle$ (meV)
KP_5W_{30}	0.42	0.085	0.079	0.42 ± 0.10	0.07 (0.025/0.2)	0.05 (0.02/0.13)
$NH_4P_5W_{30}$	0.49	0.33	0.39	0.53 ± 0.17	0.31 (0.1/1)	0.28 (0.09/0.83)
HP_5W_{30}	0.57	0.68	0.81	0.54 ± 0.19	0.61 (0.15/2.4)	0.51 (0.14/1.86)
$TBAP_5W_{30}$	0.69	2.0	1.0	0.66 ± 0.16	1 (0.24/4.3)	0.99 (0.25/3.8)

of magnitude of these parameters are observed from the analysis of the mean $\bar{I}$–V, the statistical analysis of the full dataset, and using both the SEL and TVS methods, making the experimental observations conclusive.

Discussion

The low-bias conductance of the P_5W_{30}-based MJs increases by a factor of ∼100 from the K^+ to the TBA^+ cations (Fig. 3b and c). However, the weak increase of the energy position of the LUMO (by a factor of ∼1.6, Fig. 3d and Table 2) should have induced a decrease of the current due to a higher electron energy barrier ($\varepsilon_0 - \varepsilon_F$) at the molecule/electrode interface. A factor of ∼4.5 is estimated from eqn (1) assuming the same molecule/electrode coupling energy for simplicity ($\Gamma_1 = \Gamma_2 = 0.1$ meV) in the simulated I–V curves (Fig. S16 in the ESI†). The increase of the measured current is clearly related to the large increase (a factor of ∼20, Fig. 3d and Table 2) of the molecule/electrode coupling energy. We examine several hypotheses to explain these results. The trend observed in solution for the size-depending behavior of the alkali salts of POMs is barely transposable: indeed, a positive shift of the reduction potential (which would correspond here to a stabilization of the LUMO and a decrease of ε_0) and a greater electron transfer rate to POMs associated with larger alkali metal cations were ascribed to an increase of the ion pairing energy related to a decrease of the cation solvation and the formation of more intimate cation/anion pairs.[22] Although we cannot completely exclude the presence of some remaining solvent molecules in our MJs, solvation is not really relevant here. In a recent theoretical report, the efficiency of cations to compensate for the charging of a hexavanadate POM has been addressed by simultaneous addition of extra cations and electrons: in the gas phase, Li^+ and H^+ were found to be the most efficient, followed by $NH_4{}^+$ and K^+.[43] Although the origin of this effect was not further discussed, it could similarly impact the electron transport across the MJs. Last but not least, the tetrabutylammonium cation is very different from the other cations used in this study, and because of its volume and lower charge density, it is the softest cation of the series.

Among many factors, the energy level alignment in the MJs (the LUMO of the P_5W_{30} POM with respect to the electrode Fermi energy) may depend on the interface dipole. A larger TBA counterion could probably induce a larger local dipole (larger distance between the positive and negative charges), and if we assume that the counterions are mostly inserted between the POM monolayer and the electrode (due to steric hindrance, *vide supra* the thickness measurements), then a global dipole could exist at the interface with an orientation leading to an upward larger LUMO offset from the Fermi level due to the dipole-induced vacuum level shift (Fig. S17 in the ESI†). In contrast, smaller cations create weaker dipoles randomly arranged around the POM,[44] resulting in a weaker (or even negligible) average dipole at the interface, and thus a weaker LUMO shift. Note that we cannot exclude, at this stage without further theoretical explorations, that the atomistic details of the POM/electrode contact configuration also play a role (as also known in many other MJs). In the case of the $W_{18}O_{54}(SO_3)^{2-}$ based MJs,[26] a change by a factor of *ca.* 4 in the amplitude of the current and a variation of the LUMO between *ca.* 0.4 and 1.2 eV were theoretically predicted with respect to whether the POM was oriented with its long axis perpendicular or horizontal between the electrodes and how (atomic configuration) the POM was connected to the Au electrode. From the thickness measurements (*vide supra*), we also suggest possible different orientations of the POMs, and thus further detailed calculations (out of the scope of this work) are needed to reach a conclusion.

The evolution of the molecule/electrode coupling energy is most intriguing. Nevertheless, it has been recently demonstrated that the counterion can mediate the intermolecular electron transfer between two adjacent and nearby POMs,[45] leading to a possible POM–cation–POM electron conduction channel. In the situation schematically depicted above for the case of the TBA^+ counterion (Fig. S17 in the ESI†), we extrapolate that the same kind of mechanism could enhance the POM–cation–electrode electronic coupling, compared to a more random organization around the POMs for the other counterions (Fig. S17†). Moreover, the fact that the POM/electrode interaction also depends on the nature of the counterions, was observed from the STM images of a single POM deposited on a metal surface. In this experiment, the size of the electron cloud density measured by STM largely extends the geometric size of the POM due to the hybridization of the POM and the counterion with the metal surface, with a stronger hybridization with a TBA^+ cation rather than the POM encapsulated in a cyclodextrin cage (cation free).[25] This hybridization is also the key factor for fixing the molecule/electrode energy coupling in the SEL model (eqn (1)). Thus, we hypothesize that the TBA^+ counterion could lead to a stronger POM/electrode hybridization than the other ones. Finally, we note that our energy values with the TBA^+ counterion (ε_0 = 0.66–0.69 eV, Γ_1 and $\Gamma_2 \approx$ 1–2 meV) are of the same order as the values determined by STM experiments on a single similar Preyssler POM ($[DyP_5W_{30}O_{110}]^{12-}$) in the case of a strong molecule/electrode coupling (established by moving the STM tip in close contact to the molecule in that case): $\varepsilon_0 \approx 0.7$ eV, Γ_1 and $\Gamma_2 \approx$ 1–10 meV.[46]

At higher voltages ($|V| > 0.7$ V), the bump of the current cannot be fitted with the SEL model. We hypothesize that this "additional" current can be due to a second level entering in the energy window at higher voltages (Fig. S11 in the ESI†). Such a behavior was theoretically simulated in the case of a two-channel electron transmission in the MJs.[47] This second level is tentatively attributed to the LUMO+1 of the POMs. Our results suggest that the LUMO+1 is less sensitive to the counterions, since the currents at $|V| > 0.7$ V are less dependent on them (Fig. 3b and Fig. S10 in the ESI†). We also note that the POM samples with the NH_4^+ and H^+ countercations display slightly higher currents at +1 V than those at −1 V (Fig. S10 and Table S1 in the ESI†), while no voltage dependence asymmetry is observed at lower voltages (Fig. S9†). The mean asymmetry ratio (also known as the rectification ratio) $R = \bar{I}(+1\ V)/\bar{I}(-1\ V)$ is weak ($\approx$1.7 and $\approx$3.2 for HP_5W_{30} and $NH_4P_5W_{30}$, respectively) with a difference in log-$\bar{I}$ (log-mean current) of 0.24 for HP_5W_{30} and 0.5 for $NH_4P_5W_{30}$, smaller than log-σ (log standard deviation, in the range of 0.84–1.1). It has been pointed out that weak R values must be considered with caution without a solid statistical analysis.[48] A two-sample *t*-test on the current datasets at +1 and −1 V was used to assess if these datasets statistically and significantly differ from each other (see Section 9 in the ESI†). The *t*-test results show that the null hypothesis (the same mean value for the two datasets) can be rejected and this weak current asymmetry is statistically significant. The origin of this effect may be due to different contact geometries of the POM to the electrodes (at the atomic level) in the presence of the different counterions, with an asymmetric hybridization between the POM and the two electrodes for the LUMO+1 in the case of H^+ and NH_4^+ counterions (no asymmetry is observed at lower bias, −0.6/0.6 V, involving only the LUMO in the electron transport mechanism (Fig. 3c and Fig. S9 in the ESI†)). A similar effect was theoretically predicted for the $W_{18}O_{54}(SO_3)^{2-}$ POM with TMA (symmetric *I–V*) or Cs^+ (asymmetric *I–V*) counterions.[26] Further theoretical work (out of the scope of this work) would be necessary to clarify this point.

Conclusion

In conclusion, we have demonstrated that the electron transport properties, at the nanoscale, of P_5W_{30}-based molecular junctions depend on the nature of the counterions. From a statistical study (hundreds of *I–V* traces) using a simple analytical model derived from the Landauer–Imry–Büttiker formalism for charge transport in nanoscale devices, we have found that the energy position of the LUMO of P_5W_{30} with respect to the Fermi energy of the electrodes increases from ~0.4 eV to ~0.7 eV and that the electrode coupling energy evolves from ~0.05 to 1 meV depending on the nature of the counterion in the order from K^+, NH_4^+, H^+ to TBA^+. We have suggested that these variations could be due to a counterion-dependent POM/electrode interface dipole and a molecule/electrode hybridization mediated by the counterions. These non-trivial POM–counterion–metal electrode interactions clearly require further theoretical studies to elucidate the influence of the counterions on the electron transport properties of POM-based molecular devices.

Methods

Sample fabrication

Bottom metal electrode fabrication. Template-stripped gold (^{TS}Au) substrates were prepared according to a method previously reported[49–51] (Section 2 in the ESI†).

Self-assembled monolayers. The SAMs on ^{TS}Au were fabricated following a protocol developed and optimized in our previous works for the electrostatic immobilization of POMs on amine-terminated SAMs[17,28] (Section 2 in the ESI†).

Spectroscopic ellipsometry

The thickness of the SAMs was measured by spectroscopic ellipsometry (UVISEL ellipsometer (HORIBA), Section 3 in the ESI†).

CAFM under ambient conditions. We measured the electron transport properties at the nanoscale by CAFM (ICON, Bruker) at room temperature using a tip probe in platinum/iridium (see Section 4 in the ESI†).

Author contributions

C. H., S. R., F. V. and A. P. synthesized and characterized the POMs and fabricated the SAMs. C. H. did all the C-AFM measurements, C. H. and D. V. analyzed the data. A. P. and D. V. conceived and supervised the project. The manuscript was written by D. V. with the contributions of all the authors. All authors have given approval to the final version of the manuscript.

Conflicts of interest

The authors declare no competing financial interest.

Acknowledgements

We acknowledge the support of the CNRS (France), project neuroPOM, under a grant of the 80PRIME program. We are thankful to Dr Masahiro Sadakane for sharing his knowledge

about the preparation of the tetrabutylammonium salt of the Preyssler anion.

References

1 G. Heimel, E. Zojer, L. Romaner, J. L. Brédas and F. Stellacci, Doping molecular wires, *Nano Lett.*, 2009, **9**(7), 2559–2564.

2 C. J. Chen, M. Smeu and M. A. Ratner, Modeling ion sensing in molecular electronics, *J. Chem. Phys.*, 2014, **140**(5), 054709.

3 X. Xiao, B. Xu and N. Tao, Conductance titration of single peptide molecules, *J. Am. Chem. Soc.*, 2004, **126**, 5370–5371.

4 F. Chen, X. Li, J. Hihath, Z. Huang and N. J. Tao, Effect of anchoring groups on single-molecule conductance: comparative study of thiom-, amine-, and carboxylic-acid-terminated molecules, *J. Am. Chem. Soc.*, 2006, **128**(49), 15874–15881.

5 T. K. Tran, K. Smaali, M. Hardouin, Q. Bricaud, M. Ocafrain, P. Blanchard, S. Lenfant, S. Godey, J. Roncali and D. Vuillaume, A Crown-Ether Loop-Derivatized Oligothiophene Doubly Attached on Gold Surface as Cation-Binding Switchable Molecular Junction, *Adv. Mater.*, 2013, **25**(3), 427–431.

6 E. Mervinetsky, I. Alshanski, S. Lenfant, D. Guerin, L. Medrano Sandonas, A. Dianat, R. Gutierrez, G. Cuniberti, M. Hurevich, S. Yitzchaik, *et al.*, Electron Transport through Self-Assembled Monolayers of Tripeptides, *J. Phys. Chem. C*, 2019, **123**(14), 9600–9608.

7 H. Audi, Y. Viero, N. Alwhaibi, Z. Chen, M. Iazykov, A. Heynderickx, F. Xiao, D. Guerin, C. Krzeminski, I. M. Grace, *et al.*, Electrical molecular switch addressed by chemical stimuli, *Nanoscale*, 2020, **12**(18), 10127–10139.

8 B. Capozzi, J. Xia, O. Adak, E. J. Dell, Z. F. Liu, J. C. Taylor, J. B. Neaton, L. M. Campos and L. Venkataraman, Single-molecule diodes with high rectification ratios through environmental control, *Nat. Nanotechnol.*, 2015, **10**(6), 522–527.

9 Y. Ai, A. Kovalchuk, X. Qiu, Y. Zhang, S. Kumar, X. Wang, M. Kuhnel, K. Norgaard and R. C. Chiechi, In-Place Modulation of Rectification in Tunneling Junctions Comprising Self-Assembled Monolayers, *Nano Lett.*, 2018, **18**(12), 7552–7559.

10 P. Chandra Mondal, U. M. Tefashe and R. L. McCreery, Internal Electric Field Modulation in Molecular Electronic Devices by Atmosphere and Mobile Ions, *J. Am. Chem. Soc.*, 2018, **140**(23), 7239–7247.

11 Y. Han, C. Nickle, Z. Zhang, H. Astier, T. J. Duffin, D. Qi, Z. Wang, E. Del Barco, D. Thompson and C. A. Nijhuis, Electric-field-driven dual-functional molecular switches in tunnel junctions, *Nat. Mater.*, 2020, **19**(8), 843–848.

12 Y. Wang, Q. Zhang, H. P. A. G. Astier, C. Nickle, S. Soni, F. A. Alami, A. Borrini, Z. Zhang, C. Honnigfort, B. Braunschweig, *et al.*, Dynamic molecular switches with hysteretic negative differential conductance emulating synaptic behaviour, *Nat. Mater.*, 2022, **21**, 1403–1411.

13 Y. Zhang, L. Liu, B. Tu, B. Cui, J. Guo, X. Zhao, J. Wang and Y. Yan, An artificial synapse based on molecular junctions, *Nat. Commun.*, 2023, **14**, 247.

14 D. L. Long, R. Tsunashima and L. Cronin, Polyoxometalates: building blocks for functional nanoscale systems, *Angew. Chem., Int. Ed.*, 2010, **49**(10), 1736–1758.

15 O. Linnenberg, M. Moors, A. Notario-Estevez, X. Lopez, C. de Graaf, S. Peter, C. Baeumer, R. Waser and K. Y. Monakhov, Addressing Multiple Resistive States of Polyoxovanadates: Conductivity as a Function of Individual Molecular Redox States, *J. Am. Chem. Soc.*, 2018, **140**(48), 16635–16640.

16 M. J. Turo, L. Chen, C. E. Moore and A. M. Schimpf, Co^{2+}-Linked $[NaP_5W_{30}O_{110}]^{14-}$: A Redox-Active Metal Oxide Framework with High Electron Density, *J. Am. Chem. Soc.*, 2019, **141**(11), 4553–4557.

17 C. Huez, D. Guérin, S. Lenfant, F. Volatron, M. Calame, M. L. Perrin, A. Proust and D. Vuillaume, Redox-controlled conductance of polyoxometalate molecular junctions, *Nanoscale*, 2022, **14**, 13790.

18 C. Busche, L. Vila-Nadal, J. Yan, H. N. Miras, D. L. Long, V. P. Georgiev, A. Asenov, R. H. Pedersen, N. Gadegaard, M. M. Mirza, *et al.*, Design and fabrication of memory devices based on nanoscale polyoxometalate clusters, *Nature*, 2014, **515**(7528), 545–549.

19 H. Tanaka, M. Akai-Kasaya, A. TermehYousefi, L. Hong, L. Fu, H. Tamukoh, D. Tanaka, T. Asai and T. Ogawa, A molecular neuromorphic network device consisting of single-walled carbon nanotubes complexed with polyoxometalate, *Nat. Commun.*, 2018, **9**(1), 2693.

20 D. Banerjee, T. Kotooka, S. Azhari, Y. Usami, T. Ogawa, J. K. Gimzewski, H. Tamukoh and H. Tanaka, Emergence of In-Materio Intelligence from an Incidental Structure of a Single-Walled Carbon Nanotube–Porphyrin Polyoxometalate Random Network, *Adv. Intell. Syst.*, 2022, **4**(4), 2100145.

21 G. Zhang, Z. Y. Xiong, Y. Gong, Z. Zhu, Z. Lv, Y. Wang, J. Q. Yang, X. Xing, Z. P. Wang, J. Qin, *et al.*, Polyoxometalate Accelerated Cationic Migration for Reservoir Computing, *Adv. Funct. Mater.*, 2022, **32**, 2204721.

22 V. A. Grigoriev, D. Cheng, C. L. Hill and I. A. Weinstock, Role of Alkali Metal Cation Size in the Energy and Rate of Electron Transfer to Solvent-Separated 1:1 $[(M^+)(\text{Acceptor})]$ ($M^+ = Li^+, Na^+, K^+$) Ion Pairs, *J. Am. Chem. Soc.*, 2001, **123**(22), 5292–5307.

23 A. Misra, K. Kozma, C. Streb and M. Nyman, Beyond Charge Balance: Counter-Cations in Polyoxometalate Chemistry, *Angew. Chem., Int. Ed.*, 2020, **59**(2), 596–612.

24 K. Y. Monakhov, Implication of counter-cations for polyoxometalate-based nano-electronics, *Comments Inorg. Chem.*, 2022, 1–10.

25 F. Yang, M. Moors, D. A. Hoang, S. Schmitz, M. Rohdenburg, H. Knorke, A. Charvat, X.-B. Wang, K. Y. Monakhov and J. Warneke, On-Surface Single-Molecule Identification of Mass-Selected Cyclodextrin-

Supported Polyoxovanadates for Multistate Resistive-Switching Memory Applications, *ACS Appl. Nano Mater.*, 2022, **5**(10), 14216–14220.

26 P. Lapham, L. Vila-Nadal, L. Cronin and V. P. Georgiev, Influence of the Contact Geometry and Counterions on the Current Flow and Charge Transfer in Polyoxometalate Molecular Junctions: A Density Functional Theory Study, *J. Phys. Chem. C*, 2021, **125**(6), 3599–3610.

27 M. H. Alizadeh, S. P. Harmalker, Y. Jeannin, J. Martin-Frere and M. T. Pope, A heteropolyanion with fivefold molecular symmetry that contains a nonlabile encapsulated sodium ion. The structure and chemistry of $[NaP_5W_{30}O_{110}]^{14}$, *J. Am. Chem. Soc.*, 1985, **107**(9), 2662–2669.

28 K. Dalla Francesca, S. Lenfant, M. Laurans, F. Volatron, G. Izzet, V. Humblot, C. Methivier, D. Guerin, A. Proust and D. Vuillaume, Charge transport through redox active $[H_7P_8W_{48}O_{184}]^{33-}$ polyoxometalates self-assembled onto gold surfaces and gold nanodots, *Nanoscale*, 2019, **11**(4), 1863–1878.

29 I. Creaser, M. C. Heckel, R. J. Neitz and M. T. Pope, Rigid nonlabile polyoxometalate cryptates $[ZP_5W_{30}O_{110}]^{(15-n)-}$ that exhibit unprecedented selectivity for certain lanthanide and other multivalent cations, *Inorg. Chem.*, 1993, **32**(9), 1573–1578.

30 Y. Jeannin, J. Martin-Frere, D. J. Choi and M. T. Pope, The Sodium Pentaphosphato(V)-Triacontatungstate Anion Isolated as the Ammonium Salt, in *Inorganic Syntheses*, ed. A. P. Ginsberg, Wiley & Son, 1990, vol. 27, pp. 115–118.

31 M. Sadakane, Y. Ichi, Y. Ide and T. Sano, Thermal Stability and Acidic Strength of Preyssler-Type Phosphotungstic Acid, $H_{14}[P_5W_{30}O_{110}Na]$ and It's Catalytic Activity for Hydrolysis of Alkyl Acetates, *Z. Anorg. Allg. Chem.*, 2011, **637**(14–15), 2120–2124.

32 K. Sahiro, Y. Kawato, K. Koike, T. Sano, T. Nakai and M. Sadakane, Preyssler-type phosphotungstate is a new family of negative-staining reagents for the TEM observation of viruses, *Sci. Rep.*, 2022, **12**(1), 7554.

33 S. Datta, *Electronic transport in mesoscopic systems*, Cambridge University Press, 1995.

34 J. C. Cuevas and E. Scheer, *Molecular electronics: an introduction to theory and experiment*, World Scientific, 2010.

35 L. Grüter, F. Cheng, T. T. Heikkilä, M. T. González, F. Diederich, C. Schönenberger and M. Calame, Resonant tunnelling through a C60 molecular junction in a liquid environment, *Nanotechnology*, 2005, **16**(10), 2143–2148.

36 J. P. Bourgoin, D. Vuillaume, M. Goffman and A. Filoramo, Molecular Electronics, in *Nanoscience*, ed. C. Dupas, P. Houdy and M. Lahmani, Springer, 2007.

37 J. Brunner, *Gaining Microscopic Insight into Molecular Junctions by Transport Experiments*, PhD thesis, Basel University, 2013.

38 J. M. Beebe, B. Kim, J. W. Gadzuk, C. Daniel Frisbie and J. G. Kushmerick, Transition from Direct Tunneling to Field Emission in Metal-Molecule-Metal Junctions, *Phys. Rev. Lett.*, 2006, **97**(2), 026801.

39 J. M. Beebe, B. Kim, C. D. Frisbie and J. G. Kushmerick, Measuring Relative Barrier Heights in Molecular Electronic Junctions with Transition Voltage Spectroscopy, *ACS Nano*, 2008, **2**(5), 827–832.

40 E. H. Huisman, C. M. Guédon, B. J. van Wees and S. J. van der Molen, Interpretation of Transition Voltage Spectroscopy, *Nano Lett.*, 2009, **9**(11), 3909–3913.

41 F. Mirjani, J. M. Thijssen and S. J. van der Molen, Advantages and limitations of transition voltage spectroscopy: A theoretical analysis, *Phys. Rev. B: Condens. Matter Mater. Phys.*, 2011, **84**(11), 115402.

42 I. Bâldea, Ambipolar transition voltage spectroscopy: Analytical results and experimental agreement, *Phys. Rev. B: Condens. Matter Mater. Phys.*, 2012, **85**(3), 035442.

43 A. S. Sorokina, D. A. Ryndyk, K. Y. Monakhov and T. Heine, What is the maximum charge uptake of Lindqvist-type polyoxovanadates in organic-inorganic heterostructures?, *Phys. Chem. Chem. Phys.*, 2022, **24**(43), 26848–26852.

44 J. A. Fernández, X. López, C. Bo, C. de Graaf, E. J. Baerends and J. M. Poblet, Polyoxometalates with Internal Cavities: Redox Activity, Basicity, and Cation Encapsulation in $[X^{n+}P_5W_{30}O_{110}]^{(15-n)-}$ Preyssler Complexes, with X = Na^+, Ca^{2+}, Y^{3+}, La^{3+}, Ce^{3+}, and Th^{4+}, *J. Am. Chem. Soc.*, 2007, **129**(40), 12244–12253.

45 I. Werner, J. Griebel, A. Masip-Sanchez, X. Lopez, K. Zaleski, P. Kozlowski, A. Kahnt, M. Boerner, Z. Warneke, J. Warneke, *et al.*, Hybrid Molecular Magnets with Lanthanide- and Countercation-Mediated Interfacial Electron Transfer between Phthalocyanine and Polyoxovanadate, *Inorg. Chem.*, 2023, **62**, 3761–3775.

46 S. Sherif, G. Rubio-Bollinger, E. Pinilla-Cienfuegos, E. Coronado, J. C. Cuevas and N. Agrait, Current rectification in a single molecule diode: the role of electrode coupling, *Nanotechnology*, 2015, **26**(29), 291001.

47 A. Migliore and A. Nitzan, Nonlinear Charge Transport in Redox Molecular Junctions: A Marcus Perspective, *ACS Nano*, 2011, **5**(8), 6669–6685.

48 C. Nijhuis, W. Reus and G. Whitesides, Molecular Rectification in Metal–SAM–Metal Oxide–Metal Junctions, *J. Am. Chem. Soc.*, 2009, **131**(49), 17814–17827.

49 M. Hegner, P. Wagner and G. Semenza, Ultralarge atomically flat template-stripped Au surfaces for scanning probe microscopy, *Surf. Sci.*, 1993, **291**, 39–46.

50 E. Weiss, R. Chiechi, G. Kaufman, J. Kriebel, Z. Li, M. Duati, M. Rampi and G. Whitesides, Influence of defects on the electrical characteristics of mercury-drop junctions: self-assembled monolayers of n-alkanethiolates on rough and smooth silver, *J. Am. Chem. Soc.*, 2007, **129**(14), 4336–4349.

51 E. A. Weiss, G. K. Kaufman, J. K. Kriebel, Z. Li, R. Schalek and G. M. Whitesides, Si/SiO_2-Templated Formation of Ultraflat Metal Surfaces on Glass, Polymer, and Solder Supports: Their Use as Substrates for Self-Assembled Monolayers, *Langmuir*, 2007, **23**(19), 9686–9694.